# Supporting Information

## Multilayered Inorganic-Organic Microdisks as Ideal Carriers for High Magnetothermal Actuation: Assembling Ferrimagnetic Nanoparticles Devoid of Dipolar Interactions.

*Idoia Castellanos Rubio*, Rahul Munshi, Yueling Qin, David B. Eason, Iñaki Orue, Maite Insausti and Arnd Pralle**

## Table of Contents

**Photolithography**

Figure S1: Positive photoresist (hole-pattern).

Figure S2: Negative photoresist (pillar-pattern).

**$Fe_3O_4$ NP density and agglomeration degree on microdisks**

Figure S3. SEM micrographs of Figure 3 at lower magnification.

Figure S4. Sample prepared with $Fe_3O_4$ NPs of 14.4±1.6 nm in diameter.

**Magnetic Measurements**

Figure S5. Ms determination ($A \cdot m^2/kg_{Fe3O4}$) of the MNPs: Thermogravimetric measurement of $Fe_3O_4$ F-MNPs in powder and M(H) curve at RT.

Figure S6. ZFC/FC curves at 0.8 kA/m of $Fe_3O_4$ F-MNPs.

Figure S7. FORC curves presented in the insets of Figure 5 (a, b, c).

Figure S8. (a, b, c) 2D projection of the FORC distributions of samples h, i and j.

Figure S9. M/Ms obtained by DCD and IRM conditions and Henkel plots.

**SAR Measurements**

Figure S10. Temperature rise in $Fe_3O_4$@PMAO NP colloid during 10 s alternating magnetic field application.

**Normalized fluorescence change vs temperature**

Figure S11. Thermal calibration plot of Alexa 647 dye

**Supplementary Methods** (Cell culture, Microdisks loading on cells and Image acquisition)

**Photolithography**

Attempts of fabricating polymeric microdisks loaded with MNPs using different approaches:

Positive photoresist (hole-pattern)

In this method a positive photoresist (S1818) was used so as to obtain a hole-pattern (by prebaking the photoresist at 115 ºC for 60 s, using custom designed chromium on quartz photomask with clear circles of 8 μm in diameter, UV exposure time of 15 s and development of 25 s with MF-319), see **Figure S1** a. Then the polyelectrolytes were sprayed layer by layer (LbL) onto the pattern at pH~3. Once the photoresist pattern was dissolved, the multilayer (ML) structure that had filled the holes stayed on the substrate while the multilayer on top of the photoresist was released giving rise to polymeric microdisks. The ML structure is composed of 3 regions:

1) The release region is composed of PMAO (Polymethacrylic acid) and PVOP (Polyvinylpyrrolidone) which assemble by H bonds. At pH>6 the PMAO deprotonates enough to cause the disassembling of this first region and the release of the remaining ML.
2) The intermediate region is form by electrostatic interactions between the strong polyelectrolytes PSS (polysodium 4-styrenesulfonate) and PDAC (polydiallyl-dimethylammonium chloride).
3) The payload region is form by electrostatic interactions between $Fe_3O_4$ NPs@PMAO and PAH (polyallylamine hydrochloride).

Total thickness of the polymeric ML shown in **Figure S1 b** $[(PMAA/PVOP)_{60}(PSS/PDAC)_{30}]$ was around 400 nm (~2.2 nm/monolayer) measured by profilometer. Bibliography suggests [S1] that the release region thickness has to be at least ~250-300 nm in order to achieve successful lift

off. Therefore, the fabrication process requires very long spraying times (>2 hours). Moreover, the need of having to spray the NP colloid at pH~3 provokes NP clustering. These NP agglomerations connect the ML with the photoresist and cause the detachment of the whole system in some areas when the resist is getting dissolved (**Figure S1** c). Moreover, the dissolution of the release region, i.e. the lift-off process, in the remaining microdisks is not quantitative as it is shown in Figure 1 of the paper. Consequently, this approach was discarded.

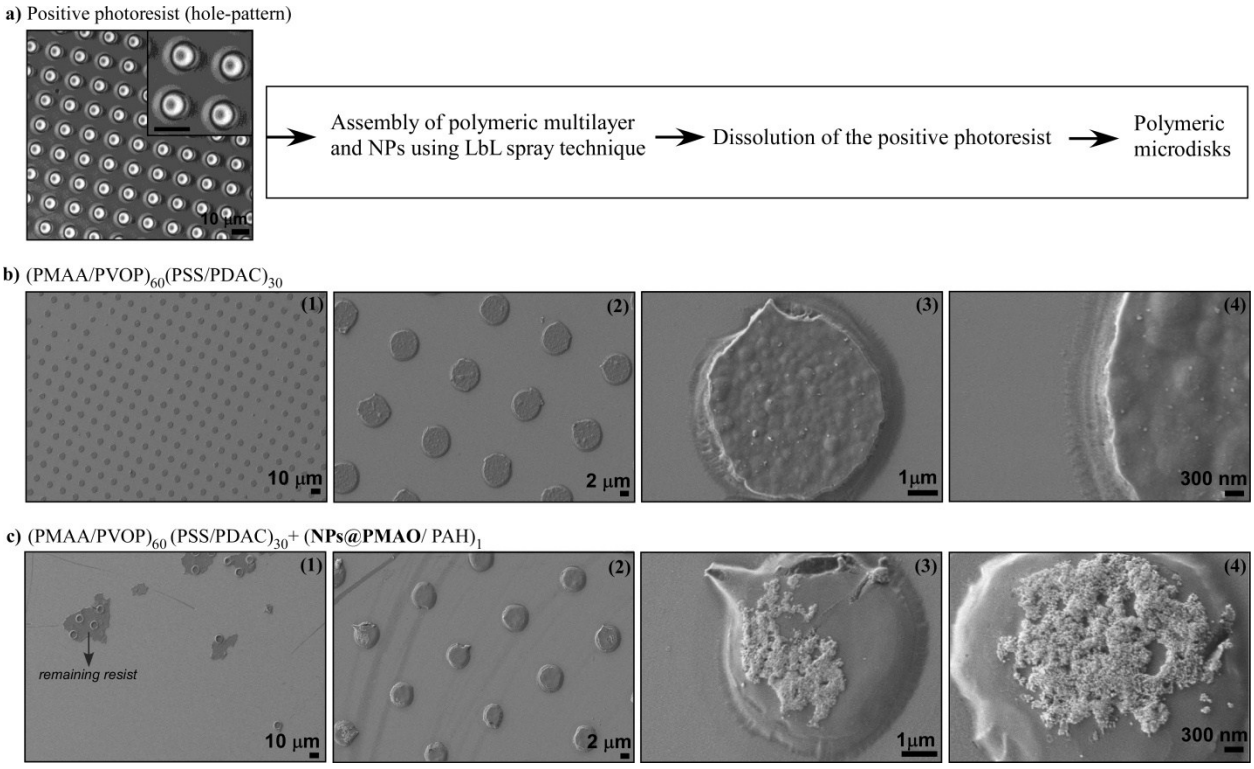


**Figure S1**. **(a)** Optical micrograph of the obtained hole-pattern by S1818 photoresist and the scheme of the *positive photoresist approach*. **(1, 2, 3, 4)** SEM micrographs at different magnifications of two samples after dissolving the positive photoresist. **(b)** A sample that was prepared alternating polymeric monolayers [$(PMAA/PVOP)_{60}(PSS/PDAC)_{30}$] and **(c)** same preparation as a) but adding $(Fe_3O_4NPs@PMAO/PAH)_1$ bilayer on the top. It can be observed how NPs form clusters in the areas where microdisks were remained.

Negative photoresist (pillar-pattern)

In this second attempt a negative photoresist (KL 1607) was chosen to make a pillar-pattern (**Figure S2**) with the same photomask that was used in the previous approach (the resist was prebaked at 110 ºC for 60 s, exposed to UV for 20 s and developed in MF-26A during 10 s). The polymeric ML structure was sprayed onto the pattern and the KL 1607 pillars were meant to be used as a sacrificial layer. Nevertheless, the sidewalls of the pillars got covered by the polyelectrolytes and NPs (**Figure S2** b); thus, it was not possible to release the ML heterostructure from the substrate. Although the preparation conditions were modified in order to obtain pillars with undercut, the results were not successful enough to get a quantitative lift off.

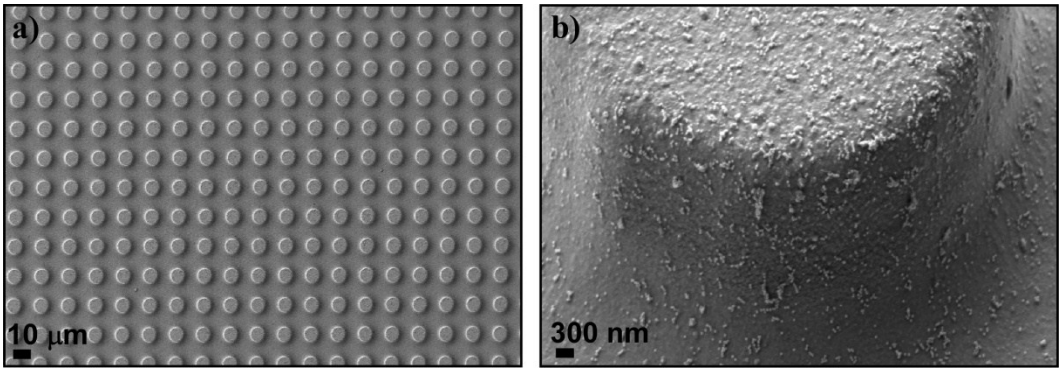


**Figure S2. (a,b)** SEM micrographs showing a result with the *negative photoresist approach* at different magnifications**.** KL 1607 negative resist was used in order to get pillars, there was no need of using low pH in this approach and, therefore, the $Fe_3O_4$ NPs were assembled more homogeneously. However, the multilayer heterostructure completely covered the sidewalls of the resist pillars and the lift off became impossible even with very thin multilayer structures (<20nm thickness).

**$Fe_3O_4$ NP density and agglomeration degree on microdisks**

**Figure S3** shows in lower magnification the samples discussed in the Figure 5 of the main paper.

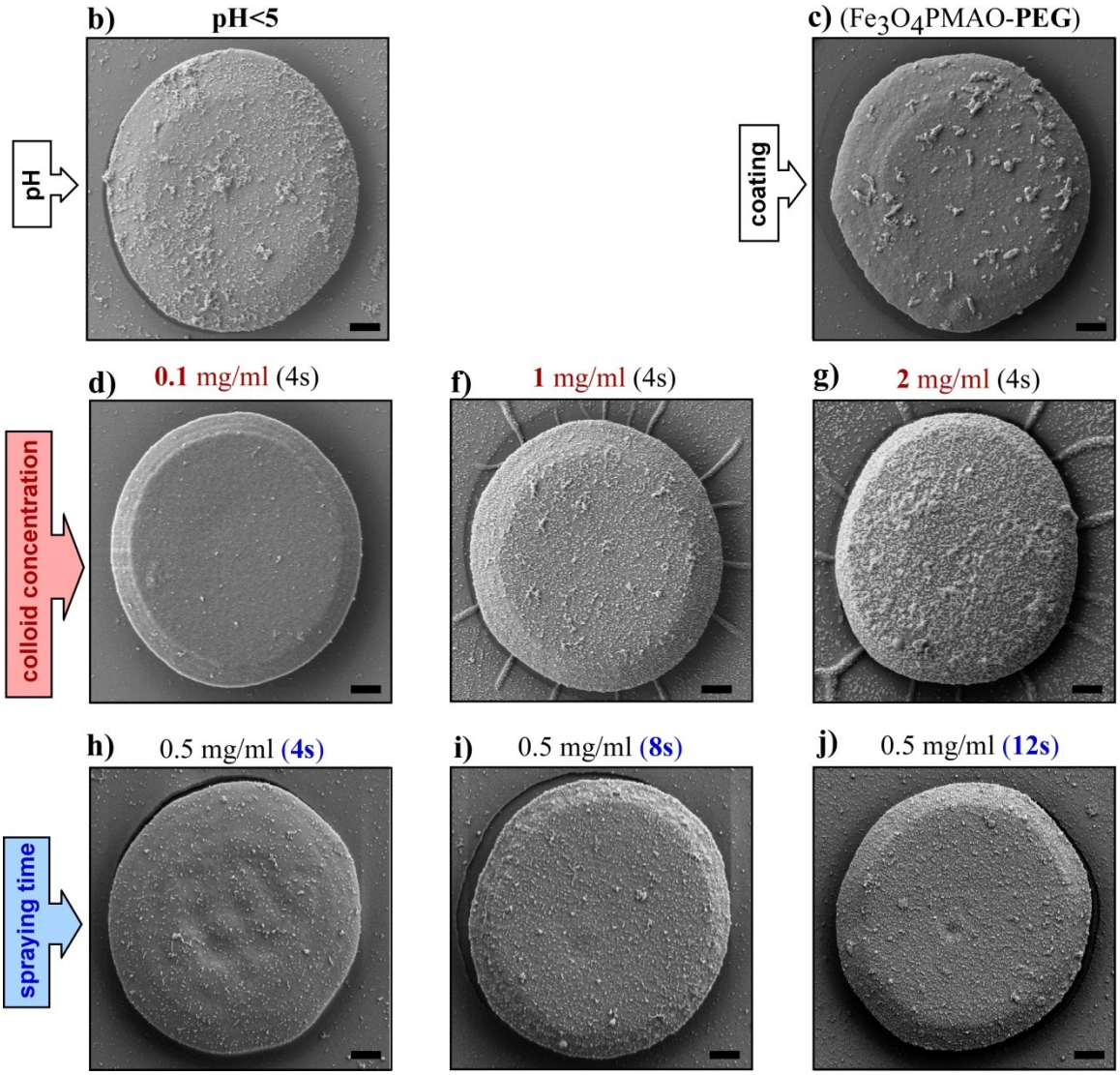


**Figure S3.** SEM micrographs of the samples presented in Figure 5 at lower magnification. The corresponding F-MNP density (measured in 5 different areas): **(d)** 24 ± 4 NPs/μm$^2$; **(f)** 190 ± 20 NPs/μm$^2$; **(g)** 520 ± 120 NPs/μm$^2$; **(h)** 45 ± 11 NPs/μm$^2$; **(i)** 84 ± 16 NPs/μm$^2$ and **(j)** 110 ± 8 NPs/μm$^2$.

The sample presented in **Figure S4** was prepared by spraying a colloid of $Fe_3O_4$@PMAO SP-MNPs of 1 mg/ml (at pH=6.5) for 4 s. As it can be observed, smaller MNPs (SP-MNPs) can be assembled at high density (>800 NPs/$\mu m^2$) with very low degree of agglomeration using a NP colloid concentration of 1 mg/ml. Therefore, getting a homogeneous assembly of non-magnetic NPs by this approach seems to be very easy to attain.

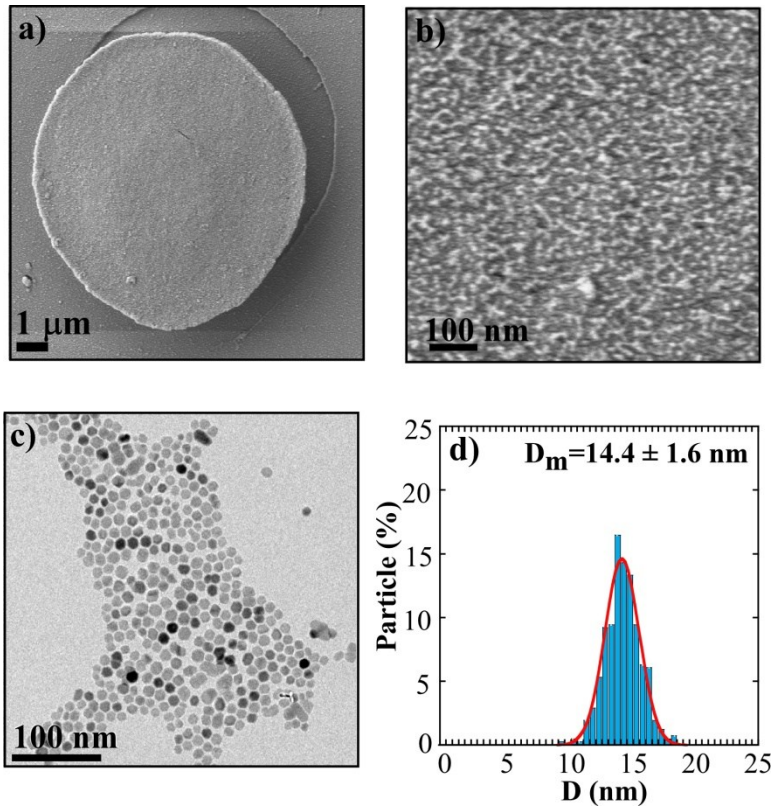


**Figure S4. (a, b)** SEM micrographs of a sample prepared with $Fe_3O_4$ SP-MNPs of 14.4±1.6 nm in diameter (at 14 kX and 90 kX, respectively). **(c, d)** TEM image of $Fe_3O_4$ NPs used and the corresponding size distribution.

**Magnetic Characterization**

M(H) curve at RT of $Fe_3O_4$ ferromagnetic NPs in powder sample.

The saturation magnetization (Ms) of the $Fe_3O_4$ F-MNPs used in this study was obtained by measuring directly a dried colloid of as-synthesized F-MNPs (powder sample). A thermogravimetric measurement of the powder was carried out to determine the organic mass percent (9.7%) in the sample (**Figure S5** a) and to normalize the Ms per mass unit of inorganic matter (Ms = 76 A·m2/kg $_{Fe3O4}$, **Figure S5** b).

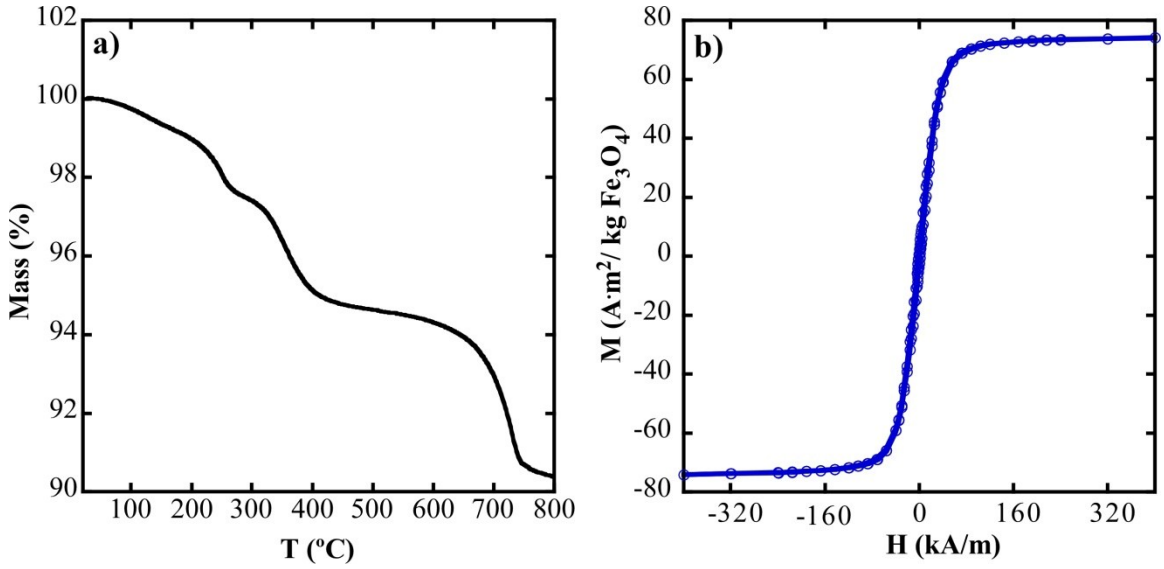


**Figure S5**. **(a)** Thermogravimetric measurements in Ar up to 800 ºC of $Fe_3O_4$ F-MNPs in powder. **(b)** M(H) curve at RT corresponding to the powder sample of $Fe_3O_4$ F-MNPs.

ZFC/FC curves at 0.8 kA/m of $Fe_3O_4$ ferromagnetic NPs.

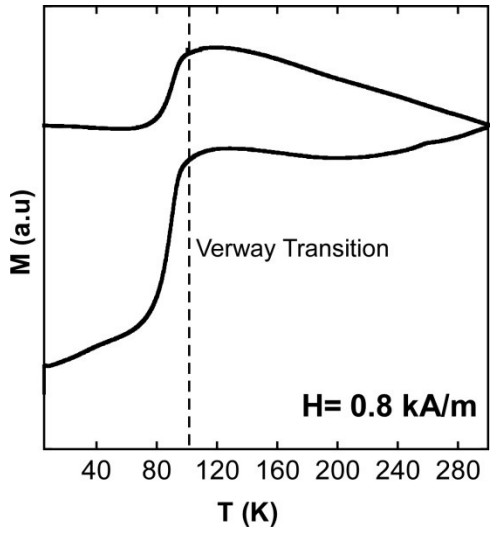


**Figure S6**. ZFC/FC magnetization curves corresponding to $Fe_3O_4$ F-MNPs.

First Order Reversal Curves (FORCS) measurements.

In this measurement protocol, the sample is subjected to magnetic loops between the same maximum *positive* field ($+H_{max}$) and progressively smaller minimum fields up to reach the total major loop (from $-H_{max}$ to $+H_{max}$) (**Figure S7**). FORC curves correspond to the increasing field branch of such loops and so they start at gradually lower magnetic fields, which are usually called reversal fields ($H_R$). Such reversal fields are scaled by the same step as applied magnetic field, and therefore, magnetization changes can be easily calculated from the derivatives of magnetization relative to both, applied field H and reversal field $H_R$. In this particular case, maximum fields is of 120 kA/m and field step is 1.2 kA/m. Because the sensitivity of the magnetization measurements in the FORCs should be at least 1000 times better than the maximum magnetic moment of the sample, FORC measurements have been performed in a continuous multilayer that was sprayed simultaneously with the photolithographic pattern. Note that in the SQUID magnetometer used for these measurements, relative sensitivity is about

$1 \cdot 10^{-11}$ $Am^2$ and therefore minimum magnetic moment of the whole sample should be above $1 \cdot 10^{-8}$ $Am^2$ in order to get a reliable 3D distribution map of magnetization switching events.

In addition to the very visual 3D representation shown in Figure 7 of the manuscript, it is also useful to represent the 2D projection of FORC distribution over the plane given by interacting bias field ($H_b$) and local coercive field ($H_c$) variables (**Figure S8**). In these plots, contour lines enclose regions where magnetization switching events are taking place more frequently. In the very weak interacting sample (h), in **Figure S8** a, contour lines strongly concentrate along the axis where interacting dipolar field is strictly zero. It is also very clear that in the sample with higher NP agglomeration (c), these lines spread out of the $H_b$=0 axis so indicating the onset of significant dipolar interactions (**Figure S8** c).

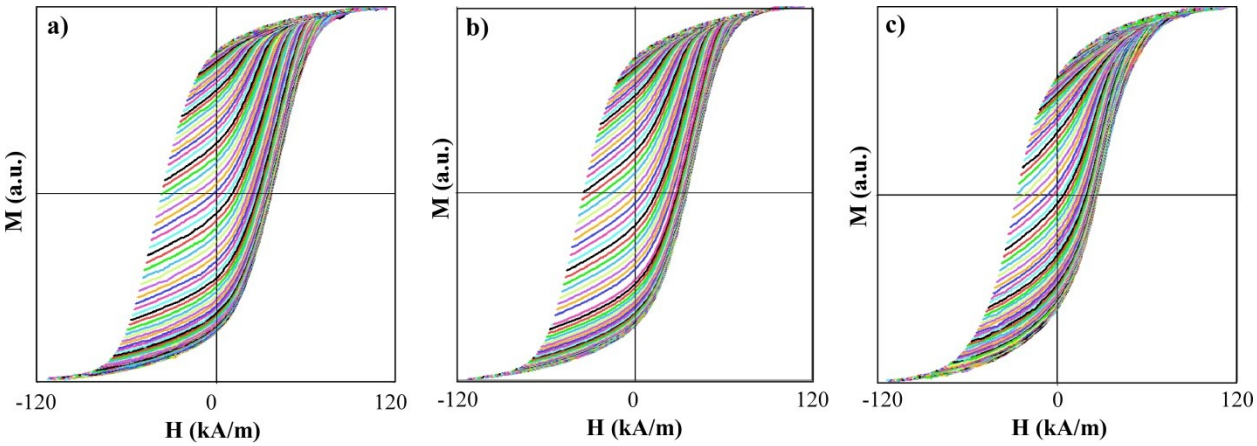


**Figure S7. (a, b, c)** FORC curves presented in the insets of Figure 7 (a, b, c), respectively.

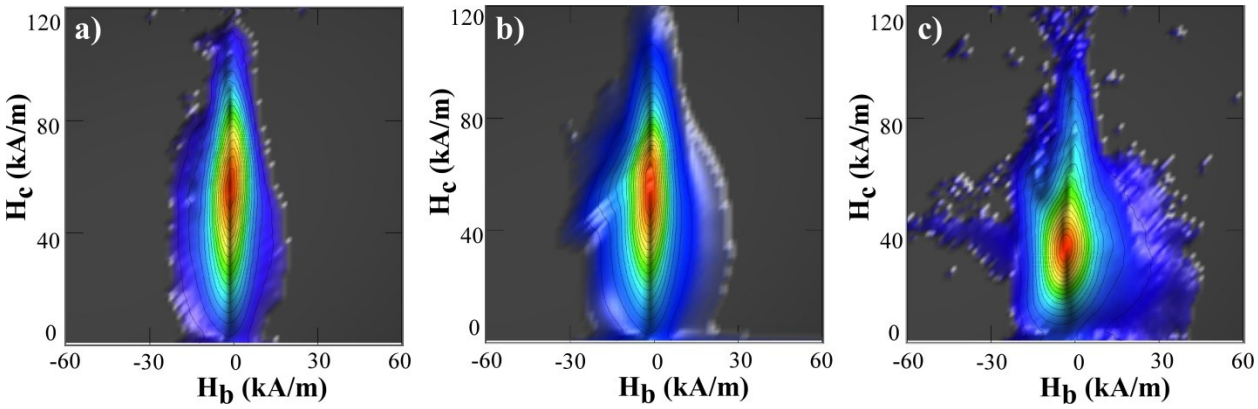


**Figure S8. (a, b, c)** 2D projection of the FORC distributions of samples h, f and c, respectively.

**Henkel plot constructions**

In magnetic nanoparticle systems, a common way to visualize and quantify the interparticle interactions is the construction of the so-called Henkel plot, where two remanent magnetizations obtained by a different approach are plotted against each other.

In this XY representation ordinates commonly correspond to the reduced Demagnetization Remanence ($M_{DCD}/M_R = m_{DCD}$) and abscissas to the reduced Isothermal Remanence ( $M_{IRM}/M_R = m_{IRM}$), following the standard denomination, where $M_R$ is the maximum remanent magnetization (close to 0.5 times the saturation magnetization in non-interacting uniaxial single domains oriented at random). It is important to understand what these variables are really accounting for. Both of them are basically quantifying how many irreversible magnetization processes take place under the application of an external field pulse of increasing amplitude: during a single measurement the magnetic field is successively switched on and off and then the remanence magnetization is measured. The difference between $M_{IRM}$ and $M_{DCD}$ relies on the initial state of the nanoparticle assembly: for obtaining $M_{IRM}$ curve, the sample is demagnetized

prior to the application of magnetic pulses of increasing amplitude, while the assembly is magnetized with a large field applied in the opposite direction to the field pulse for obtaining each $M_{DCD}$ point. In this way one can construct two plots of remanence magnetizations, $M_{IRM}$ and $M_{DCD}$, as a function of the field pulse amplitude, such as those presented in Figure S9 (a) and S9 (b). Note that $M_{IRM}$ start from 0 (demagnetized state) and saturates at the maximum remanent magnetization $M_R \sim 0.5 M_S$, while $M_{DCD}$ starts at $-M_R$ (reversal magnetized state) and finishes at $M_R$ (magnetized in the direction of positive pulses).

For systems composed of single magnetic domains, a demagnetized sample means that magnetic moment vectors are pointing towards any direction of space with equal probability; terminal point of such vectors or *states* are spread equally over north and south hemispheres. In this case, a magnetic pulse directed, let´s say, along the North pole will prompt a number of particle magnetization switchings from equivalent "south" (down) minima to "north" (up) minima. Once beyond a certain magnetic intensity threshold, down states are removed and $M_{IRM}$ remains constant and equal to $M_R$. If the magnetization reversal at each "object" is an independent process (dipolar interactions negligible or isolated objects), the same magnetic pulse but applied to a sample magnetized downwards (used for measuring $m_{DCD}$) produce twice as many irreversible jumps as before. This is just because the density of *states* in the south hemisphere in a magnetized state is also double the density of *states* in the demagnetized one. It means that in the non-Interacting particle approximation $m_{IRM}$ and $m_{DCD}$ should verify a quite simple linear relation:

$$-m_{DCD}^{nonI} = 2 - 2m_{DCD}^{nonI} \qquad (S1)$$

Equation (S1) is represented by the black colored dashed line in the insets of Figures S9 (a) and S9 (b). However if single domains are indeed interacting to each other (via dipolar or exchange mechanisms), the relation between $m_{DCD}$ and $m_{IRM}$ is expected to deviate from that given in equation S1. In our Henkel plots (insets), sample h matches approximately to the non-Interacting prediction while sample c deviates significantly from it. Just to quantify this deviation, it is convenient to define a new variable $\delta m$ as the difference between the experimental $m_{DCD}$ and the non-interacting limit given by equation S1:

$$\delta m = m_{DCD} - (2 - 2m_{IRM}). \quad \text{(S2)}$$

Depending on the sign of $\delta m$, interaction promotes demagnetizing ($\delta m < 0$) or magnetizing ( $\delta m > 0$) effects, as discussed elsewhere in the literature [S2,S3,S4] Demagnetizing/magnetizing effects means that antiparallel/parallel configurations are energetically favored by interactions and so would affect magnetized state (and then to $m_{DCD}$) to a greater degree than demagnetized one ($m_{IRM}$). In our case, as observed in Figure S9 (c), $\delta m$ is negative for sample h and c, what is usually explained as due to random dipolar interactions in 3D assemblies that favor antiparallel configurations of neighboring single magnetic domains. The important point is that the strength of $\delta m$ in sample c is by far greater than in sample h, which shows almost negligible influence from dipolar interactions. This analysis is an agreement with conclusions extracted from the FORC distribution obtained at 50 K, namely, that NPs' clustering affects the magnetic behavior of individual NPs in sample c in much higher degree than in sample h.

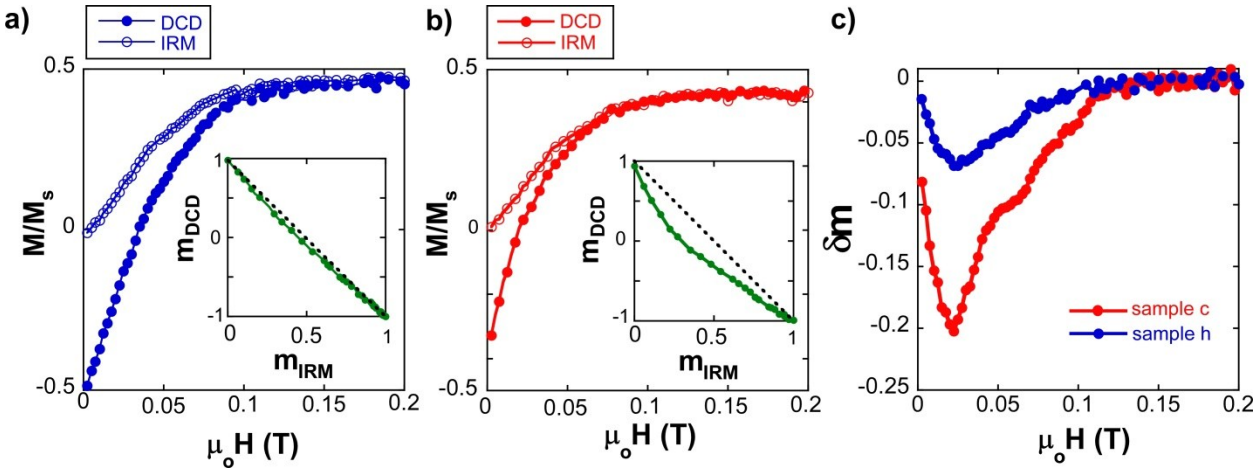


**Figure S9**. Remanent reduced magnetization obtained by DCD and IRM conditions **(a)** in sample h and **(b)** in sample c. Insets show the corresponding Henkel plots of samples h and c. **(c)** Representation of $\delta m$ as a function of the amplitude of the magnetic field pulse.

**SAR measurements**

Specific Absortion Rate (SAR) measurements on $Fe_3O_4$ ferromagnetic NP colloid suspension were performed using a custom build, water-cooled coil driven by a power supply from MSI Automation Inc. (Wichita, Kansas). The coil's mean radius was 2.4 cm and had 6 turns. The sample temperature was recorded using a fiber optic temperature sensor (T1S-03-WNO-B05) and an analogue to digital converter (ReFlex) from Neoptix (Quebec, Canada). The sample holder had double walled glass, sealed with a plastic cap. Annular air gaps between the glass walls of the sample holder and between the sample holder and the coil ensured near adiabatic conditions for small temperature changes. The aqueous suspension of the $Fe_3O_4$@PMAO F-MNPs was subjected to magnetic field for 10 seconds and the temperature rise was simultaneously recorded. The mean magnetic flux density along the sample column (1 cm) was 36 kA/m at 412.5 kHz.

The *dT/dt* values were obtained from the slope of a linear fit to the data for the first degree change in temperature. SLP was calculated by using Equation S2:

$$SLP = \frac{C_{water} \cdot \rho_{water} dT}{c_{np} \quad dt} \qquad \text{(S2)}$$

where, C is the specific heat of water (4.18 J/g$^{o}$C), ρ is the density of water (1 g/cm$^3$) and $c_{np}$ is the concentration of the NP colloid in $g_{Fe3O4}$/ml. **Figure S10** shows the *dT/dt* plot corresponding to a colloid of $c_{np}$= 2·10$^{-3}$$g_{Fe3O4}$/ml (16 NP/μm$^3$) at 36 kA/m and 412.5 kHz. The measurement was repeated three times which gave a SAR of 2140 ± 50 W/$g_{Fe3O4}$

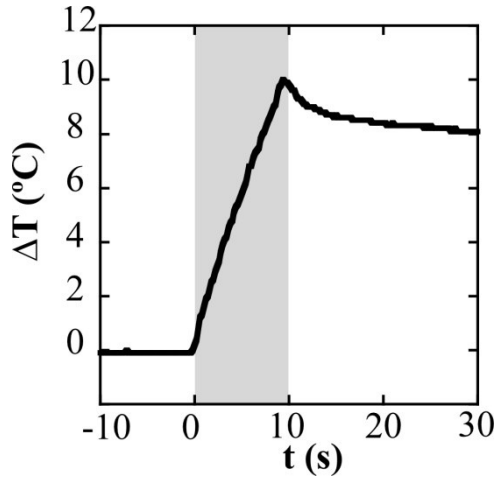


**Figure S10**. Temperature rise and subsequent cooling during a 10 s AMF (36 kA/m at 412.5 kHz) application in a $Fe_3O_4$@PMAO F-MNP colloid (2 mg/ml).

**Normalized fluorescence intensity change vs temperature change**

**Figure S11** shows mean ± sem of normalized fluorescence signal measured from Alexa 647 dye on the microdisks. Fluorescence quenching with increasing temperature can be clearly seen. Linear fit of data points is shown with the dashed line. The slope of the plot is -0.0046 ± 0.0002

ºC$^{-1}$, implying that there is a 0.46% dip in fluorescence intensity for every degree Centigrade change in temperature.

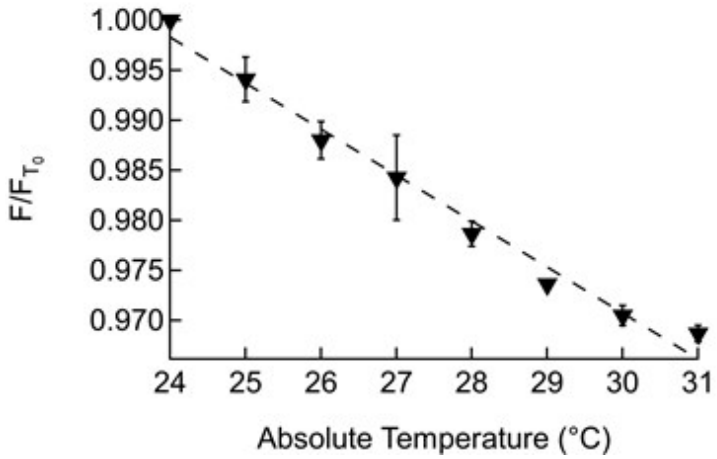


**Figure S11.** Thermal calibration plot of Alexa 647 dye (Thermo Fisher Cat. No. A20006). The calibration was done on the dye attached to nanoparticles within the microdisks. Left axis shows mean ± sem fluorescence signal normalized to 24 °C signal.

**Cell Culture**

HEK 293 cell line was a gift from Dr. Cohen (Harvard). The cells were stably expressing channelrhodhopsin 2 in the cell membrane, with a GFP tag. The cells were cultured and passaged per published protocol.[S5] For imaging, all cells were grown in 12 mm glass coverslips coated with poly-L-Lysine, for adherence.

Hippocampal cultures were obtained from Sprague-Dawley rat fetuses (E 16) and maintained according to published protocol.[S6] For imaging, day *in-vitro* (DIV) 14 cultures were used.

For fixation, the media in the wells was replaced with ice cold 4% Paraformaldehyde (PFA) in Phosphate buffer solution (PBS) and the cells were incubated for 20 minutes. The cells were then washed in PBS and stored at 4 ºC, until used.

**Microdisk loading on cells**

Living (or PFA fixed) cells were biotinylated (1:200) by adding 1 µL biotin (EZ-link Sulfo-NHS-Biotin, ThermoFisher Scientific), dissolved in DMSO to 200 µL PBS. The cells were washed three times with PBS prior to this step. Incubation time was 20 – 30 minutes at room temperature. Excess biotin was then washed off and a suspension containing microdisks (in PBS) was then added. Gentle pipetting of the buffer solution was done 2 – 3 times, followed by a 10 minutes incubation, to ensure that most microdisks attached to the cells. For preparation of slides for confocal microscopy, the coverslips were placed on glass slides and were sealed with enamel.

**Fluorescence microscopy of cell loaded microdisks**

Epifluorescence microscopy was done with an inverted microscope (Zeiss Axio Observer A 1.0m), fitted with 40x (NA = 0.75, air) objective lens (Zeiss), mounted on a feedback controlled autofocus mount (MotionX corp.). Mounted LEDs (Thorlabs) with appropriate filter set and collimator lenses (Aspheric condenser lenses, Thorlabs) were used for fluorophore excitation (M470L3 for GFP; M505L3 for Rhodamine123; M625L3 for Alexa647). The coverslips were mounted on a plastic sample holder (ALA scientific) and placed in a manual (Thorlabs) or computer controlled motorized x-y stage (Märzhäuser-Wetzlar) for microscopy. Image acquisition was done with Andor Neo sCMOS camera, controlled by Andor Solis software or µManager software. For long term membrane attachment test, microdisks were loaded to HEK293 cells and images were snapped at various hour marks. The dish was not disturbed during the entire duration of the experiment and focus was held in place by the Autofocus. A computer controlled XY stage (Märzhäuser Wetzlar, controlled by Tango desktop) was used to reposition ROIs during acquisition. Illumination was only done during imaging and the entire experiment was done at room temperature.

**Magnetic field generation and fluorescence thermometry**

Alternating magnetic field was generated in an insulated coil made out of an insulated hollow ¼ inch copper tubing. The coil was driven by a 7.5 kW hyperthermia power system acquired from MSI Automation, Wichita, KS, USA and was constantly cooled with flowing water. Magnetic field measurements were done with a Fluxtrol AC magnetic field probe. For heating microdisks on cells, the coil was placed over the microscope stage, with a Delrin sample holder (ALA Scientific) right underneath it. Focal shifts, during magnetic heating were compensated for in the real time by a commercial autofocus (Motion X corp.).

**Supplemental References**


[S1] A. J. Swiston, C. Cheng, S. H. Um, D. J. Irvine, R. E. Cohen, M. F. Rubner, *Nano Lett*., 2008, **8**, 4446.

[S2] K. O'Grady and R. W. Chantrell, in *Magn. Prop. Fine Part., Proc. Int. Workshop Stud. Magn. Prop. Fine Part. Their Relevance Mater. Sci.*, North-Holland, 1992, pp. 93–102.

[S3] D. Peddis, C. Cannas, G. Piccaluga, E. Agostinelli and D. Fiorani, *Nanotechnology*, 2010, **21**, 125705/1-125705/10.

[S4] S. Laureti, G. Varvaro, A. M. Testa, D. Fiorani, E. Agostinelli, G. Piccaluga, A. Musinu, A. Ardu and D. Peddis, *Nanotechnology*, 2010, **21**, 315701/1-315701/6.

[S5] J. Park, C. a. Werley, V. Venkatachalam, J. M. Kralj, S. D. Dib-Hajj, S. G. Waxman, A. E. Cohen, *PLoS One,* 2013, **8**, e85221.

[S6] R. Munshi, S. M. Qadri, Q. Zhang, I. C. Rubio, P. del Pino, A. Pralle, *Elife,* 2017, **6**, 1.